Investigations on the mixed Jahn-Teller system (Tb_x, Dy_{1-x})VO_4. II. Birefringence measurements in the orthorhombic phases

1990 J. Phys.: Condens. Matter 2 1097

(http://iopscience.iop.org/0953-8984/2/5/004)

J. Phys.: Condens. Matter **2** (1990) 1097–1112. Printed in the UK

Investigations on the mixed Jahn–Teller system $(Tb_x,Dy_{1-x})VO_4$: II. Birefringence measurements in the orthorhombic phases†

G Hess

Physikalisches Institut, Universität Karlsruhe (TH), PO Box 6980, D-7500 Karlsruhe 1, Federal Republic of Germany

Received 2 May 1989, in final form 22 August 1989

Abstract. Measurements of the linear birefringence at different wavelengths λ in the visible part of the spectrum are presented for the two orthorhombic phases of the mixed Jahn–Teller system $(Tb_x,Dy_{1-x})VO_4$. These two phases have different crystal structures according to different distortion types of the pure substances. For low concentrations x, the crystals distort like $DyVO_4$, and the measured curves are proportional to each other for different λ. For high x, however, where the crystals distort like $TbVO_4$, the measured curves are not proportional to each other and are not proportional to the order parameter (distortion). The measured curves are explained by calculations within the frame of a modified mean-field formalism including higher-order contributions to the birefringence.

1. Introduction

In the preceding paper [1], henceforth referred to as I, the phase diagram and the distortion types of the mixed Jahn–Teller system $(Tb_x,Dy_{1-x})VO_4$ were established (figure 1 of paper I). Three low-temperature phases were observed: two orthorhombic phases with a crystal structure and a distortion type like the pure substances and a monoclinic phase in which the distortion types of the pure substances superimpose.

Birefringence is a very suitable tool in the study of structural phase transitions as it can be measured with great accuracy [2]. It is generally related either to the order parameter or to the square of the order parameter, depending on the experimental set-up [3]. In ferroelastic structural phase transitions, in first approximation the order parameter is proportional to the macroscopic distortion [4].

In the mixed system $(Tb_x,Dy_{1-x})VO_4$, two distortion types, Γ_3^+ and Γ_4^+ (see paper I), and therefore two order parameters occur. The distortions are designed as e_X and e_A, respectively. In the orthorhombic phases, one of these order parameters is equal to zero. In this paper we report on birefringence measurements in the orthorhombic phases of $(Tb_x,Dy_{1-x})VO_4$, which were performed at different wavelengths λ in the visible part of the spectrum. The birefringence in the monoclinic phase and special problems of measuring the birefringence of monoclinic crystals are discussed in the following paper [5], henceforth designed as III.

† This paper is dedicated to Professor H G Kahle on the occasion of his 65th birthday.

0953-8984/90/051097 + 16 $03.50

The measured curves are interpreted within the frame of a modified mean-field approximation (MFA) for the Tb-rich compounds and of a modified compressible Ising (CI) model for the Dy-rich compounds. For details of the Jahn–Teller effect in $(Tb_x,Dy_{1-x})VO_4$ and in the pure substances, especially for the calculation of the order parameters (distortions e_X and e_A), we refer to paper I and references therein.

2. Experimental details

2.1. Crystals

Crystals of concentrations $x = 0.0, 0.1, \ldots, 0.9, 1.0$ and additionally $x = 0.35$ and 0.45 were flux-grown [6]. They were cut perpendicular to the tetragonal (= high-temperature) c axis and polished to a thickness d of 0.5 mm $\leqslant d \leqslant$ 1.7 mm. The polished surfaces were parallel to each other within 10′ and the deviations of the normals of these surfaces from the c direction were smaller than 30′.

2.2. Optical set-up

The crystal was placed in an exchange-gas cryostat with optical windows. The temperature was measured by means of a calibrated carbon resistor. To avoid crystallographic domains in the low-temperature phases, a constant magnetic field of $B \simeq$ 0.1 T was applied in the distortion direction [7–11] by means of a conventional electromagnet.

The crystal was irradiated with monochromatic light of different wavelengths λ parallel to the tetragonal c direction, i.e. the birefringence of the morphic tetragonal phase was zero. The birefringence was measured with a modulation technique [12] and a computer-controlled compensation of the corresponding phase difference by means of a Babinet–Soleil compensator. Modulator, compensator and crystal were placed between crossed polarisers. The axes of the optical indicatrix of modulator, compensator and crystal in the orthorhombic phases were parallel to each other and at 45° to the polarisation direction. Details of the measuring method have been published elsewhere [13, 14]. The measured quantities are the birefringence $\delta n_X = n_x - n_y$ for the crystals distorting like $TbVO_4$ and $\delta n_A = n_a - n_b$ for the crystals distorting like $DyVO_4$, both as functions of the temperature T. Thus δn_X is related to the Γ_3^+ distortion (e_X) and δn_A is related to the Γ_4^+ distortion (e_A).

The light sources used were a red He–Ne laser (λ = 632.8 nm), a green He–Ne laser (λ = 543.5 nm) and a high-pressure Hg lamp with emission lines at λ = 436, 547, 578 and 691 nm. Owing to a periodic defect in the drive of the compensator the accuracy of the measurements was limited to $\Delta(\delta n) = 1.5 \times 10^{-6}$.

3. Theory of the birefringence

3.1. General considerations

Changes of the electric polarisability caused by different mechanisms of excitation are the reason for the birefringence in the rare-earth vanadates [15–17]. These mechanisms are (i) localised excitations of the rare-earth cations from the 4f configuration to higher configurations, (ii) charge-transfer excitations of the vanadate anion and (iii) excitations

of optical phonons. Usually the latter is neglected compared with the other two mechanisms. Following the formalism of Becker and Gehring [15], the birefringences δn_X and δn_A are calculated in the following subsections for excitations of the Tb^{3+} and Dy^{3+} ions in diluted $TbVO_4$ and diluted $DyVO_4$ for both Jahn–Teller distortions Γ_3^+ and Γ_4^+. In all cases the corresponding contributions to the birefringence have to be parametrised.

In continuation of earlier work [14], contributions of the vanadate ions are designed as $A_i(\omega)$, contributions of the Tb^{3+} ions as $B_i(\omega)$ and contributions of the Dy^{3+} ions as $E_i(\omega)$. These parameters are a condensation of the individual contribution of each excitation containing dipole matrix elements M_{ge} changed by the phase transition and frequency-dependent terms of the form $(\omega_{ge} + \delta_{ge})/[(\omega_{ge} + \delta_{ge}) - \omega]$. Here ω_{ge} denotes the frequency difference of a crystal-field state $|g\rangle$ of the ground term and a crystal-field state $|e\rangle$ of an excited term in the undisturbed high-temperature phase, δ_{ge} is the change of the separation of these states in the low-temperature phase and ω is the measured frequency.

3.2. *Diluted Tb^{3+}, Γ_3^+ distortion*

The Tb^{3+} levels of the ground term $^7F_6$ populated at temperatures $T \gtrsim T_D$ (T_D = distortion temperature) are a singlet ($|1\rangle = |\Gamma_1\rangle$) at $-\varepsilon$, a doublet ($|2, 3\rangle = |\Gamma_5\rangle$) at ε' and a further singlet ($|4\rangle = |\Gamma_3\rangle$) at $+\varepsilon$ (see paper I).

The mixing of the two doublet eigenfunctions (with mixing angle φ) and the splitting of the doublet due to the Γ_3^+ distortion were calculated in MFA. Because of the higher-order effects in the birefringence observed in this work (see § 4.1), the calculations of the excited levels and the matrix elements were carried out in perturbation theory up to the second order. The result of all these calculations is (for further details see [18])

$$\begin{aligned}\delta n_X(\omega) = x_{Tb}[&e_X(p_1 + p_4)G_1'(\omega) + e_X(p_1 - p_4)\cos(2\varphi)G_2'(\omega)\\ &+ (p_1 - p_4)\sin(2\varphi)G_3'(\omega) + (p_2 - p_3)G_4'(\omega)\\ &+ e_X(p_2 + p_3)G_5'(\omega)] + O(e_X^3).\end{aligned} \tag{1}$$

Here $x_{Tb} = x$ is the Tb concentration, the p_i are the relative populations of the four crystal-field states of the ground term and the $G_i'(\omega)$ are frequency-dependent parameters explained below. In $O(e_X^3)$ all terms proportional to e_X^3 are included without any further specification.

The parameters $G_i'(\omega)$ are concerned with transitions to excited levels in zeroth- or first-order perturbation theory and in first or second order of the Taylor expansion of $(\omega_{ge} + \delta_{ge})/[(\omega_{ge} + \delta_{ge})^2 - \omega^2]$ into powers of $1/(\omega_{ge}^2 - \omega^2)$. For simplicity, we use a notation (m, n) where m is the degree of the perturbation of the excited levels and n is the power of $1/(\omega_{ge}^2 - \omega^2)$.

$G_1'(\omega)$ and $G_2'(\omega)$ contain contributions of excitations out of the two ground-state singlets to excited doublets in (1,1) and (0,2). $G_3'(\omega)$ is caused by an interference term in $|M_{ge}|^2$ containing a product of matrix elements with the different ground-state singlets in (0,1). $G_4'(\omega)$ or $G_5'(\omega)$ represent the contributions of doublet-to-singlet transitions in (0,1) or in (1,1) and (0,2), respectively. $O(e_X^3)$ contains contributions of, for example, doublet-to-singlet transitions in (0,3), (1,2) and (2,1).

The relative populations p_i and their sums and differences are non-trivial functions of the distortion e_X. It therefore seemed reasonable to separate the four-level system of

the Tb^{3+} ion into two two-level systems, which are considered separately as was done earlier [16].

3.2.1. Doublet components of the ground state. The system with the doublet ground state corresponds to $TmVO_4$ diluted with a Jahn–Teller (JT)-inactive rare-earth ion. In this case $p_2 + p_3 = 1$ and in MFA according to paper I,

$$p_2 - p_3 = \tanh\left(\frac{H_0' e_X}{kT}\right).$$

e_X is calculated self-consistently with the quantities H_0', V_0, c_0 and μ as defined in I

$$e_X = f_X(e_X) = x\left(\frac{V_0 c_0}{\mu}\right)^{1/2} \tanh\left(\frac{H_0' e_X}{kT}\right). \tag{2}$$

Then the birefringence (equation (1) with $G_1' = G_2' = G_3' = 0$) becomes

$$\delta n_X(\omega) = e_X\left(\frac{V_0 c_0}{\mu}\right)^{1/2} G_4'(\omega) + x e_X G_5'(\omega). \tag{3}$$

At first sight it may be surprising that the birefringence contains a part that is not explicitly dependent on the concentration. The reason is that the population difference, $p_2 - p_3$, of the two doublet components is proportional to the distortion, but the distortion is scaled with $1/e_{max}(x) \sim 1/x$ in the diluted case. The crucial quantities determining the birefringence are the relative populations p_i and not the distortion. The first term of equation (3) appears already in zeroth-order perturbation of the excited singlets. The second term of (3), which is explicitly concentration-dependent, follows from first-order perturbation of the excited singlets.

3.2.2. Singlet components of the ground state. For a system of interacting singlets without the additional doublet, $p_1 + p_4 = 1$ and in MFA

$$p_1 - p_4 = \tanh\left(\frac{[(H_0' e_X)^2 + \varepsilon^2]^{1/2}}{kT}\right).$$

With a self-consistent calculation of e_X similar to above, one gets from equation (1) with $G_4' = G_5' = 0$

$$\delta n_X(\omega) = x e_X G_1'(\omega) + e_X \frac{\varepsilon}{J_0'} G_2'(\omega) + e_X\left(\frac{V_0 c_0}{\mu}\right)^{1/2} G_3'(\omega). \tag{4}$$

(J_0' is defined in equation (7) of paper I.) Also in this case some terms are explicitly concentration-dependent and some are not.

3.2.3. Whole four-level system. Extensive calculations for diluted $TbVO_4$ have shown that at high Tb concentrations x the proportionality between birefringence and distortion holds within 5% down to about $0.5T_D$ and at $x = 0.5$ still down to $0.8T_D$ [14]. Therefore it seems justified to combine the results of the last two subsections to obtain the birefringence caused by the whole four-level system of Tb^{3+} in diluted $TbVO_4$. Thus the birefringence consists of a first contribution that is explicitly dependent on the concentration and a second one that is independent of the concentration. Including a contribution proportional to e_X^3 it is

$$\delta n_X(\omega) = x_{Tb} e_X B_1(\omega) + e_X B_2(\omega) + e_X^3 B_3(x_{Tb}, \omega). \tag{5}$$

This *ansatz* is justified only for $TbVO_4$ diluted with a Jahn–Teller-inactive rare-earth

ion. That includes a dilution with Dy^{3+}, because $DyVO_4$ does not noticeably couple to a Γ_3^+ distortion [19]. It is not justified for a dilution with Tm^{3+}, however. The problem for $(Tb_x,Tm_{1-x})VO_4$ [14] is the following. The relative populations in equation (1) cannot be expressed as simple functions of the distortion, because the equation for the self-consistent calculation of the distortion always contains a contribution of the Tm^{3+} ion. Although it may be shown nevertheless that the birefringence is proportional to the distortion, nothing can be stated about the dependence of the birefringence on the concentration.

According to the above discussion, the parameters $B_1(\omega)$ and $B_2(\omega)$ contain, in leading order perturbation theory, terms proportional to both $1/(\omega_{ge}^2 - \omega^2)$ and $1/(\omega_{ge}^2 - \omega^2)^2$.

3.3. Diluted Tb^{3+}, Γ_4^+ distortion

The Tb^{3+} contribution to the birefringence δn_A caused by a Γ_4^+ distortion may be treated similarly to the past section. In this case, however, the two singlets do not interact. Because Tb^{3+} is not Jahn–Teller-active for this distortion, it is assumed, supported by spectroscopic investigations (see paper I), that the ground-state doublet does not split. Then the birefringence is

$$\delta n_A(\omega) = x_{Tb} e_A[(p_1 + p_4)B_4(\omega) + (p_1 - p_4)B_5(\omega) + (p_2 + p_3)B_6(\omega)]. \tag{6}$$

In the calculation of the relative populations p_i, care has to be taken whether the Tb^{3+} levels are independent of temperature or whether they depend on T, due to an additional Γ_3^+ distortion. Possible differences of these two cases are discussed in § 4.2. Contributions proportional to e_A^3 are not considered, because they could not be detected in the experiments. There are no contributions that are not explicitly dependent on the concentration. The reason for this is that Tb^{3+} is not noticeably Jahn–Teller-active for the Γ_4^+ distortion. Then the populations p_i are dependent neither on the distortion e_A nor on the concentration.

3.4. Diluted Dy^{3+}, Γ_4^+ distortion

The Dy^{3+} levels of the ground state $^6H_{15/2}$ occupied at temperatures $T \gtrsim T_D$ are two Kramers doublets, $|1\rangle = |\Gamma_6\rangle$ and $|2\rangle = |\Gamma_7\rangle$ with a separation of $2\Delta_0$.

Parametrising the results of a calculation considering the ground state in MFA modified with the compressible Ising model (see paper I) and the excited states in first-order perturbation theory, the Dy^{3+} contribution to the birefringence δn_A in diluted $DyVO_4$ is given by

$$\delta n_A(\omega) = e_A E_1(\omega) + x_{Dy} e_A E_2(\omega) \tag{7}$$

where $x_{Dy} = 1 - x_{Tb} = 1 - x$ is the Dy concentration. Contributions proportional to e_A^3 are not considered since none have been observed experimentally. So the dependence on the order parameter is the same as in a calculation in which the excited states were taken to be unperturbed [17]. Again there is a contribution that is not explicitly dependent on the concentration. This contribution results from transitions to the unperturbed part of the excited states. The contribution that depends explicitly on x_{Dy}, however, results from transitions to the perturbed part of the excited states.

3.5. Diluted Dy^{3+}, Γ_3^+ distortion

For this distortion Dy^{3+} is not noticeably Jahn–Teller-active. A change of the energies of the two ground-state Kramers doublets is not observed (see paper I), but in this case these levels may mix in first-order perturbation theory. Because $p_1 + p_2 = 1$ and $p_1 - p_2 = \tanh(\Delta_0/kT)$, the birefringence including a contribution proportional to e_X^3 from second-order perturbation reads

$$\delta n_X(\omega) = x_{Dy} e_X [E_3(\omega) + \tanh(\Delta_0/kT) E_4(\omega)] + e_X^3 E_5(x_{Dy}, \omega). \tag{8}$$

3.6. Contributions of the vanadate ion

Assuming the vanadate ion to be a non-Kramers ion (closed shell) and further assuming a singlet state as the sole ground state, the results of § 3.2 can be applied independently of the distortion type because the vanadate ion is not Jahn–Teller-active for Γ_3^+ and Γ_4^+ distortions. The birefringence is thus proportional to the distortion, as already derived from symmetry considerations [15]. Including a term proportional to e_X^3 the birefringence for the Γ_3^+ distortion is

$$\delta n_X(\omega) = e_X A_1(\omega) + e_X^3 A_2(\omega) \tag{9}$$

and for the Γ_4^+ distortion

$$\delta n_A(\omega) = e_A A_3(\omega). \tag{10}$$

The calculations showed that the parameters $A_1(\omega)$ and $A_3(\omega)$ can be expressed in first order of the perturbation and in second order of the expansion of $(\omega_{ge} + \delta_{ge})/[(\omega_{ge} + \delta_{ge})^2 - \omega^2]$ into powers of $1/(\omega_{ge}^2 - \omega^2)$ as

$$A_{1/3}(\omega) = \frac{1}{2\bar{n}(\omega)} \sum_D \frac{\delta_D(\omega_D^2 + \omega^2)|M_D|^2}{(\omega_D^2 - \omega^2)^2}. \tag{11}$$

Here the summation goes over all excited doublets $|D\rangle$, $\bar{n}(\omega)$ is a mean refractive index, ω_D is the frequency difference of the ground state to the excited doublet, δ_D is half the doublet splitting caused by the respective distortion and M_D is proportional to the respective dipole matrix element in x or a polarisation. In next-order perturbation (mixing of the excited doublets) terms of first power in $1/(\omega_D^2 - \omega^2)$ contribute.

3.7. Birefringence and pre-strains

The birefringence might be changed if the crystal contains pre-strains with a distribution $p(e_v)$ according to equation (20) of paper I. Then the birefringence becomes

$$\delta n(e) = \int \delta n(e, e_v) p(e_v)\, \mathrm{d}e_v. \tag{12}$$

For Γ_3^+ distorted $(Tb_x,Dy_{1-x})VO_4$ this does not lead to changes in the calculated temperature dependence of the birefringence (in contrast to $(Tb_x,Tm_{1-x})VO_4$ [14]). For Γ_4^+ distorted $(Tb_x,Dy_{1-x})VO_4$ the corresponding changes are not important.

It seems worth mentioning that precursor tails (i.e. a smearing-out of the birefringence curves for $T \geqslant T_D$) as often observed in birefringence measurements (e.g. [20–24]) are not the consequence of a symmetrical pre-strain distribution if the birefringence is an odd function of strain and order parameter. The functional dependence between birefringence and strain (which remains zero for $T \geqslant T_D$; see paper I, § 4.1.2) does not change, as can easily be shown. An unsymmetrical pre-strain distribution, however, indeed causes the birefringence curve to smear out near T_D in the same way as it does a uniform stress or an applied magnetic field. If the birefringence is proportional to the square of the order parameter (e.g. [22, 23]), fluctuations become more important and cause the birefringence always to smear out.

3.8. *Total birefringence of the mixed system $(Tb_x,Dy_{1-x})VO_4$*

The birefringence of the mixed system is the sum of the contributions of the preceding sections. It is given as a function of the wavelength λ rather than of the frequency ω.

For Γ_3^+ distorted crystals, equations (5), (8) and (9) yield

$$\delta n_X(x,\lambda) = e_X A_1(\lambda) + e_X^3 A_2(\lambda) + x e_X B_1(\lambda) + e_X B_2(\lambda) + e_X^3 B_3(x,\lambda) + (1-x) e_X [E_3(\lambda) + \tanh(\Delta_0/kT) E_4(\lambda)] + e_X^3 E_5(x,\lambda). \tag{13}$$

Arranging into powers of e_X and scaling to the maximum distortion e_0 of $TbVO_4$, the birefringence is given by

$$\delta n_X(x,\lambda) = \frac{e_X}{e_0} L(x,\lambda) + \left(\frac{e_X}{e_0}\right)^3 K(x,\lambda) + (1-x)\frac{e_X}{e_0} \tanh\left(\frac{\Delta_0}{kT}\right) E_4'(\lambda). \tag{14}$$

Apart from the temperature T itself, the only temperature-dependent quantity on the right-hand side of this equation is the distortion $e_X(T)$. In addition to the linear and cubic parts in $e_X(T)$ with the parameters L and K, respectively, there is a contribution from the Dy^{3+} ions with a more complex dependence on T. In the parameters L and K contributions of the Tb^{3+} ions, the Dy^{3+} ions and the vanadate ions are included.

For Γ_4^+ distorted crystals, equations (6), (7) and (10) yield

$$\delta n_A(x,\lambda) = e_A A_3(\lambda) + e_A E_1(\lambda) + (1-x) e_A E_2(\lambda) + x e_A [(p_1+p_4) B_4(\lambda) + (p_1-p_4) B_5(\lambda) + (p_2+p_3) B_6(\lambda)]. \tag{15}$$

At temperatures around the Γ_4^+ phase transition (see § 4.2) the upper singlet (Γ_3) of Tb^{3+} is not populated ($p_4 \simeq 0$); thus $p_2 + p_3 = 1 - p_1$. So this equation may be simplified. Relating the distortion to the maximum distortion e_0 of $DyVO_4$, the birefringence is given by

$$\delta n_A(x,\lambda) = \frac{e_A}{e_0} M(x,\lambda) + x \frac{e_A}{e_0} p_1 N(\lambda). \tag{16}$$

The parameter M includes contributions of the Dy^{3+}, Tb^{3+} and vanadate ions; N obviously only relates to Tb^{3+} contributions.

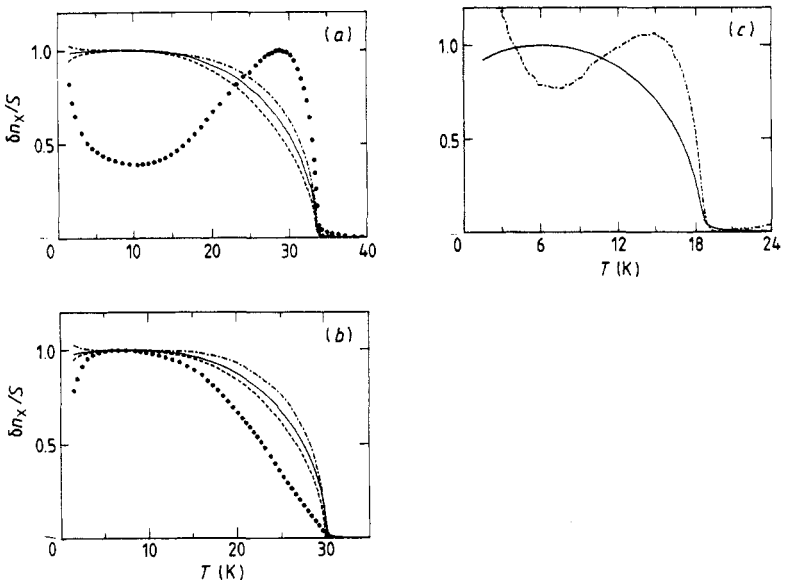

Figure 1. Measured birefringence δn_X of $(Tb_x,Dy_{1-x})VO_4$ as a function of temperature, scaled to its respective extreme value S. (*a*) Pure $TbVO_4$, $B = 0.1$ T in the distortion direction. Dots: $\lambda = 578$ nm, $S = +0.37 \times 10^{-4}$. Broken curve: $\lambda = 544$ nm, $S = -2.98 \times 10^{-4}$. Full curve: $\lambda = 436$ nm, $S = -39.0 \times 10^{-4}$. Chain curve: $\lambda = 633$ nm, $S = +3.72 \times 10^{-4}$. (*b*) $(Tb_{0.9},Dy_{0.1})VO_4$, $B = 0.1$ T in the distortion direction. Dots: $\lambda = 578$ nm, $S = -0.62 \times 10^{-4}$. Broken curve: $\lambda = 544$ nm, $S = -3.79 \times 10^{-4}$. Full curve: $\lambda = 436$ nm, $S = -35.6 \times 10^{-4}$. Chain curve: $\lambda = 633$ nm, $S = +2.47 \times 10^{-4}$. (*c*) $(Tb_{0.6},Dy_{0.4})VO_4$, $B = 0.15$ T in the distortion direction. Full curve: $\lambda = 436$ nm, $S = -24.8 \times 10^{-4}$. Chain curve: $\lambda = 633$ nm, $S = +0.106 \times 10^{-4}$. To avoid overlap of the experimental points, roughly every fifth point only is given in this figure and in figures 2, 3, 5 and 7. The curves shown in this figure are the ones corresponding to the measuring points.

4. Experiments and discussion

4.1. Γ_3^+ distorted crystals ($x \geq 0.35$)

The birefringence measurements were carried out as a function of temperature for different wavelengths for $T \geq 1.4$ K. For the mixed substances with $x = 0.35$ and $x = 0.4$, due to the Γ_4^+ distortion (see § 4.2), the measurements were confined to temperatures $T \geq 6$ K. A small magnetic field was applied in the distortion direction to avoid crystallographic domains. This was accounted for in the calculations.

Measurements on the mixed systems $(Tb_x,Tm_{1-x})VO_4$ and $(Tb_x,Yb_{1-x})VO_4$ showed a large dispersion of the birefringence in the visible region [14]. The birefringence even changes sign. This behaviour is also observed in $(Tb_x,Dy_{1-x})VO_4$. Because of this large dispersion, which will be discussed later, the measured birefringence curves are scaled to their extreme values and are shown in figure 1 for selected concentrations x. The measured curves for different wavelengths are clearly not proportional to each other. It seems worth mentioning that this non-proportionality is not a consequence of artefacts.

Neither surface effects as caused by multiple-beam reflection [25] nor crystal inhomogeneities or concentration gradients could explain the measurements, and contributions of the refractive index n_c parallel to the tetragonal c axis could be excluded by intentional misadjusting the crystal by some degrees, which did not change the measured curves in a substantial manner. On the contrary, a systematic behaviour as a function of both wavelength and concentration is observed:

(i) The scaled curves are flat if the scaling factor is negative and small, they are steep if the scaling factor is positive and small, and they are medium for great absolute values of the scaling factor.

(ii) The differences between the scaled measured curves are large for relatively large concentrations x, including pure $TbVO_4$ ($x = 1$), they become smaller with decreasing x and disappear for pure $DyVO_4$ ($x = 0$).

These observations suggest the existence of non-linear effects in the birefringence. For the experimental set-up in our measurements, one would expect a linear relation of the order parameter (distortion) and the birefringence [3]. If the linear parts of the different contributions to the birefringence (see § 3) have different signs and different dispersions, they may cancel. That means that there is some wavelength λ_0 where the linear part of the birefringence changes sign. Around λ_0, contributions to the birefringence that are of higher order in the distortion e_X are visible. From symmetry arguments as well as from an explicit calculation of the birefringence according to § 3, the next term in an expansion of δn_X in powers of e_X is proportional to e_X^3. For a test of this assumption, e_X was calculated in MFA (see paper I) with the respective magnetic field taken into consideration. Then the birefringence was fitted according to equation (14). It turned out that two parameters $L(x, \lambda)$ and $K(x, \lambda)$ were sufficient to fit the measured birefringence. The fit was consistent with $E_4'(\lambda) = 0$, i.e. the contribution due to the mixing of the Dy^{3+} ground-state doublets could be neglected compared with the other contributions. Additionally the half-width of the pre-strain distribution was used as a parameter to adjust the experimental transition temperature. In figure 2 for selected examples the fitted birefringence is compared with the measurements including the temperature dependence of the linear part $L(x, \lambda)$ (e/e_0) and the cubic part $K(x, \lambda)(e/e_0)^3$. For the yellow and red regions of the spectrum, these two parts are comparable in size (figures 2(*b*) and (*d*)). For $x = 0.9$, $\lambda = 578$ nm, the cubic part even dominates the linear one (figure 2(*c*)). The sum of these two parts yields the rather strange quasi-linear behaviour for $22\,K < T \leq T_D$. In the red (figure 2(*a*)) and green regions (not shown in the figure) of the spectrum, the cubic part is still important although here it is smaller than the linear one. Finally, in the blue region the cubic contribution can be neglected compared to the linear one and the birefringence is proportional to the order parameter for all concentrations (figure 3). With increasing dilution, the cubic part is less effective because the distortion becomes smaller. For $x = 0.4$ it is very small for all measured wavelengths.

While L depends strongly on x and λ, K is nearly independent of both concentration and wavelength ($K \simeq -0.7 \times 10^{-4}$). Figure 4 shows the dispersion of $L(x, \lambda)$ for the different concentrations; λ_0 shifts to higher wavelengths with decreasing Tb concentration. For an analysis of the dispersion of L for $TbVO_4$ we refer to [26]. In accordance with equation (13), L is a linear function of the concentration for each λ, i.e.

$$\begin{aligned} L(x, \lambda) &= e_0[A_1(\lambda) + B_2(\lambda) + E_3(\lambda)] + xe_0[B_1(\lambda) - E_3(\lambda)] \\ &= L'(\lambda) + xL''(\lambda). \end{aligned} \tag{17}$$

The coefficients $L'(\lambda)$ and $L''(\lambda)$ are given in table 1.

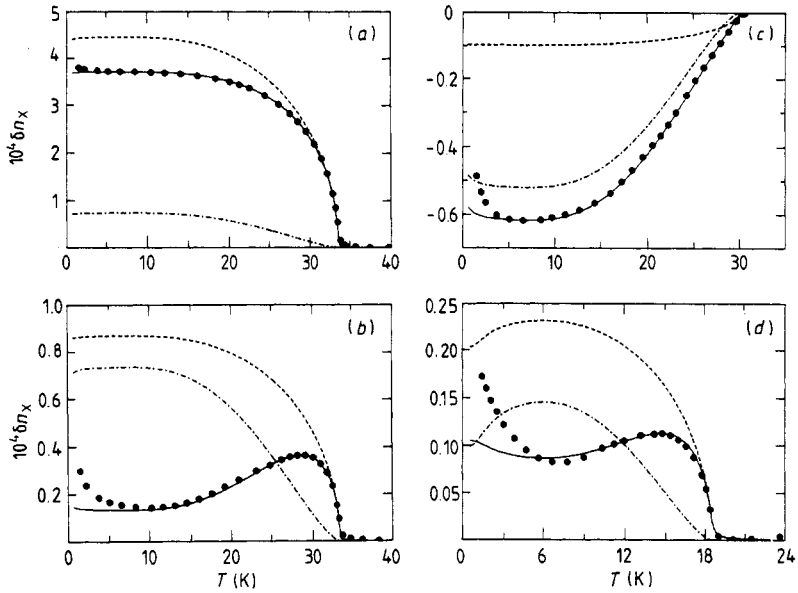

Figure 2. Measured birefringence δn_X of $(Tb_x,Dy_{1-x})VO_4$ with B in the distortion direction (dots), compared with MFA calculations and an *ansatz* according to equation (14) (full curve). Broken curve: linear part $L(e/e_0)$. Chain curve: cubic part $K(e/e_0)^3$. If $L > 0$ the cubic part has been multiplied by (-1). (*a*) $TbVO_4$, $\lambda = 633$ nm ($B = 0.1$ T); (*b*) $TbVO_4$, $\lambda = 578$ nm ($B = 0.1$ T); (*c*) $(Tb_{0.9},Dy_{0.1})VO_4$, $\lambda = 578$ nm ($B = 0.1$ T); (*d*) $(Tb_{0.6},Dy_{0.4})VO_4$, $\lambda = 633$ nm ($B = 0.15$ T).

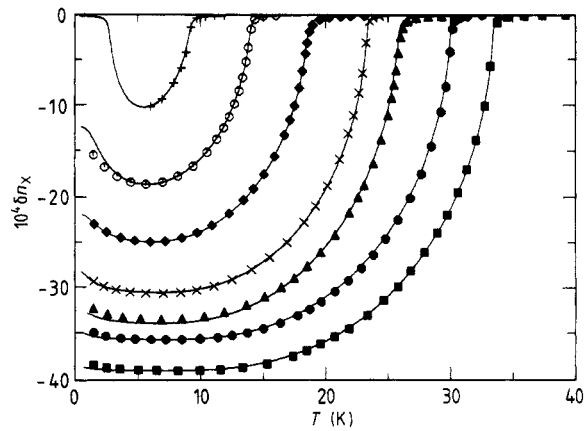

Figure 3. Measured birefringence δn_X of $(Tb_x,Dy_{1-x})VO_4$, $\lambda = 436$ nm, B in the distortion direction, compared with MFA calculations (full curves): ■, $x = 1.0$ ($B = 0.1$ T); ●, $x = 0.9$ ($B = 0.1$ T); ▲, $x = 0.8$ ($B = 0.15$ T); ×, $x = 0.71$ ($B = 0.1$ T); ◆, $x = 0.6$ ($B = 0.15$ T); ○, $x = 0.5$ ($B = 0.1$ T); +, $x = 0.4$ ($B = 0.05$ T).

Because there is a contribution of the Tb^{3+} ions to the birefringence that is not explicitly dependent on the concentration, as shown in § 3.2, a separation of this contribution and the contribution of the vanadate ions as in [14] becomes questionable.

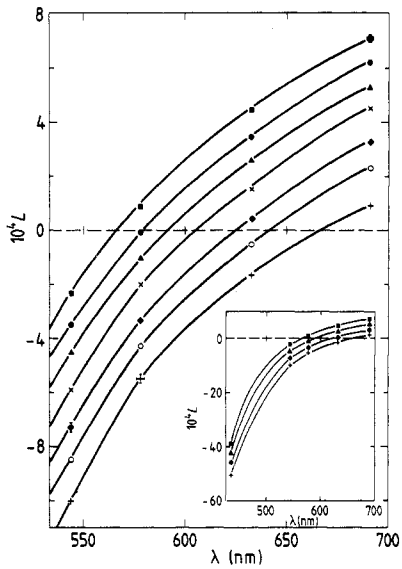

Figure 4. Parameter $L(x, \lambda)$ as a function of the wavelength λ around the zero passage. The symbols for the different concentrations are the same as in figure 3. The lines are only guides to the eye. Inset: values for the full range of measurements.

Table 1. Parameters to fit the linear part of the measured birefringence δn_X according to equation (17).

λ (nm)	691	632.8	578	543.5	436
$10^4L'(\lambda)$	-2.3 ± 0.1	-5.6 ± 0.2	-9.7 ± 0.1	-14.9 ± 0.2	-60.1 ± 0.9
$10^4L''(\lambda)$	9.5 ± 0.1	10.2 ± 0.2	10.7 ± 0.2	12.5 ± 0.2	21.9 ± 1.3

Table 2. Dy^{3+} contribution $E(\lambda)$ to the birefringence δn_X compared with the Yb^{3+} contribution $D(\lambda)$ [14].

λ (nm)	632.8	543.5	436
$10^4E(\lambda)$	8 ± 2	6 ± 2	25 ± 6
$10^4D(\lambda)$	-12 ± 2	-13 ± 3	-39 ± 11

However, the sum of these two contributions ascertained in [14] remains exact (apart from small corrections due to the cubic part, which are within the errors of the parameters given in [14]). This allowed us to determine the Dy contribution to the birefringence (see table 2).

All calculated curves agree well with the measurements for $T > T_{max}$, the temperature at which the distortion is maximal (compare, e.g. the curves for $x = 0.6$, $\lambda =$ 633 nm and $\lambda = 436$ nm, figure 2(*d*) and figure 3 (◆); $|\delta n_X|$ differs by a factor of about 100 for these wavelengths). The differences $\Delta(\delta n)$ between measured and calculated curves are smaller than 10^{-6}, except in the close vicinity of T_D where they increase to values of about 10^{-5}. This holds for all wavelengths notwithstanding the great dispersion of the measured (and the calculated) birefringence. The differences at $T \simeq T_D$ and

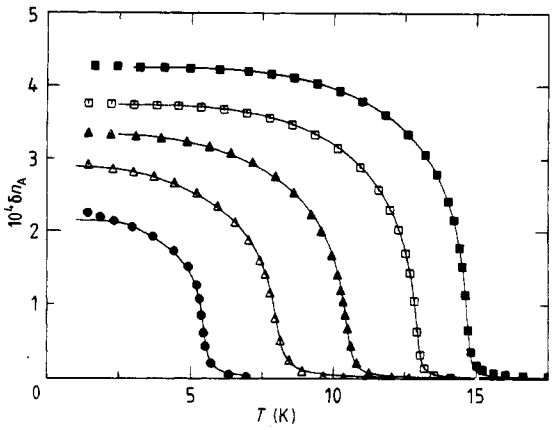

Figure 5. Measured birefringence δn_A of $(Tb_x, Dy_{1-x})VO_4$, $\lambda = 633$ nm, B in the distortion direction, compared with MFA calculations and an *ansatz* according to equation (16) (full curves): ■, $x = 0.0$ ($B = 0.1$ T); □, $x = 0.1$ ($B = 0.1$ T); ▲, $x = 0.2$ ($B = 0.1$ T); △, $x = 0.3$ ($B = 0.1$ T); ●, $x = 0.4$ ($B = 0.03$ T).

$T > T_D$ may be a result of both inaccuracies in the measured temperature and internal strains not considered in the mean-field calculation†. Furthermore, high-temperature tails may be caused by the superposition of birefringence curves resulting from regions with locally different concentrations x [24]. If one assumes a Gaussian distribution of x, a half-width $\Delta x_{1/2} \simeq 0.005$ explains the measured curves well (not shown). Thus it can be concluded that the calculations reproduce the measured curves of the birefringence within an accuracy of $\Delta(\delta n) \leqslant 10^{-5}$.

The deviations for $T < T_{max}$, on the contrary, are a direct consequence of the fact that the important quantities determining the birefringence are the relative populations and not the distortion (see § 3.2).

4.2. Γ_4^+ distorted crystals ($x \leqslant 0.4$)

The birefringence curves, which were measured on Γ_4^+ distorted crystals in a small magnetic field parallel to $\boldsymbol{a}$, are proportional to each other for different wavelengths. Scaled birefringence curves are identical within measurement accuracy. The dispersion is the same for all concentrations within the experimental errors. Therefore no contributions of a cubic term in the distortion e_A can be detected. The birefringence at $\lambda = 691$ nm is about 12% lower than at $\lambda = 436$ nm and about 3% lower than at $\lambda = 547$ nm. The birefringence for $DyVO_4$ agrees well with earlier measurements [20] apart from the value of T_D, which was 0.9 K higher in our measurements.

Because of the proportionality between the measured curves for different λ we confine ourselves to one wavelength ($\lambda = 633$ nm). In figure 5 the temperature dependence of the birefringence is shown for the mixed substances with $0.0 \leqslant x \leqslant 0.4$. Comparing the different curves, it is striking that for $x = 0.4$ (and less distinct also for $x = 0.3$) the measured birefringence does not saturate for $T \rightarrow 0$. Effects of the magnetic phase transition, which is present in the mixed substances (see paper I) as well as in pure $DyVO_4$ [27], cannot account for the observed behaviour, as the change of the birefringence caused by the magnetic phase transition is very small even for pure $DyVO_4$ ($|\Delta(\delta n_{magnet})| \leqslant 2 \times 10^{-6}$).

† The latter effect intensifies the smearing of the birefringence already present in magnetic fields (which are explicitly considered in the calculations).

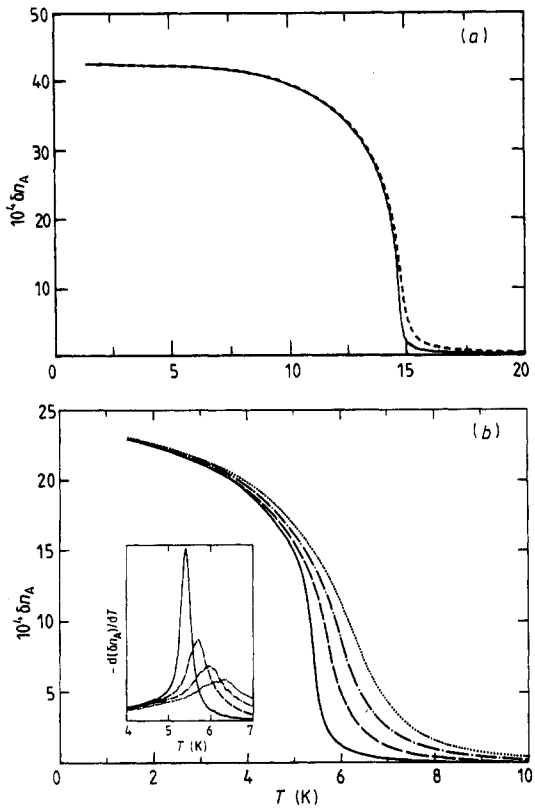

Figure 6. Measured birefringence δn_A in different magnetic fields in the distortion direction. (*a*) $DyVO_4$, $\lambda = 633$ nm. Full curve: $B = 0.1$ T. Broken curve: $B = 0.2$ T. (*b*) $(Tb_{0.4},Dy_{0.6})VO_4$, $\lambda = 544$ nm. Full curve: $B = 0.030$ T. Broken curve: $B = 0.068$ T. Chain curve: $B = 0.100$ T. Dotted curve: $B = 0.138$ T. Inset: $-d(\delta n_A)/dT$.

The birefringence in higher magnetic fields is characterised by a smearing-out of the curves for $T \simeq T_D$, which is increasing for growing concentration x (see also paper I, § 4.1.2). Whereas for pure $DyVO_4$ ($x = 0$) the differences between the curves measured for different magnetic fields are small (figure 6(*a*)), they become stronger with increasing dilution and are considerable for $x = 0.4$ (figure 6(*b*)). Even in a field as small as $B = 0.1$ T the phase transition is distinctly smeared out. This also affects the definition of the phase transition. It is defined as the extrapolation of the extremum of $d(\delta n)/dT$ to $B_{ext} = 0$. The difference of the extrapolated value and the extremum of $d(\delta n)/dT$ at $B_{ext} = 0.1$ T is already 0.8 K compared with the transition temperature $T_D = 5.2$ K. For a more detailed discussion of this problem we refer to [18]. In the limiting case of very small magnetic fields, the phase transition even for $x = 0.4$ becomes very sharp, as can be seen from the sequence of temperature derivatives in the inset of figure 6(*b*).

It might be surprising that the measured curves for $x = 0.4$ are treated in the same way as those of the crystals with greater Dy^{3+} content, although in the corresponding temperature region the crystal is additionally Γ_3^+ distorted (see § 4.1) and therefore monoclinic. Despite this, the measured δn_A curves for wavelengths in the green, yellow and red regions of the spectrum are not changed, because the δn_X birefringence relating to the Γ_3^+ distortion is small compared with δn_A. For the blue region of the spectrum ($\lambda = 436$ nm) this does not hold, however. Here effects of an interaction of the two birefringences are observed. (For a detailed discussion of the birefringence in this case see paper III.)

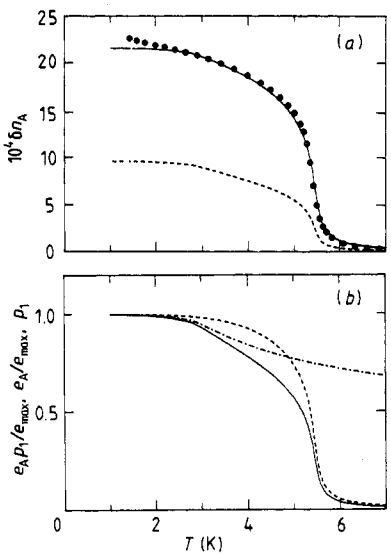

Figure 7. Temperature dependence of the birefringence δn_A of $(Tb_{0.4},Dy_{0.6})VO_4$ at λ = 633 nm, B = 0.03 T. (*a*) Measuring points (dots) compared with calculations according to equation (16) (full curve). The broken curve gives the Tb contribution $x(e_A/e_0)p_1N$. (*b*) Comparison of the Tb contribution (full curve) with the distortion e_A (broken curve) and the relative population p_1 of the lowest singlet of the Tb^{3+} ions (chain curve). The curves are scaled to their maximum values at T = 0.

Table 3. Parameters for the fit of the measured birefringence δn_A according to equation (16), λ = 633 nm. The errors in the parameters are mainly set by those in the thickness of the crystals. For the parameters $\tilde{\xi}$ and $e_{1/2}$ of the compressible Ising model, see table 3 of paper I.

x	0.0	0.1	0.2	0.3	0.35	0.4
10^4M	42.5 ± 1.0	42.5 ± 1.5	32.3 ± 1.5	28.1 ± 1.3	31.3 ± 1.3	26.5 ± 1.4
10^4N	—	0	60 ± 2	62 ± 2	59 ± 2	53 ± 2

The measured curves are compared with calculations of the distortion e_A in the compressible Ising model [28] modified with a distribution of pre-strains. For details of the calculations, see paper I. The birefringence was fitted according to equation (16) in the whole range $T_N \leqslant T \leqslant T_D$ if possible (T_N = Néel temperature). For pure $DyVO_4$ two fitting parameters were needed: the compressibility $\tilde{\xi}$ and the factor M. These values agree within the error bars with those published earlier [17]. The compressibility is even the same. Already deviations of $\Delta\tilde{\xi} = 0.01$ from the fitted value $\tilde{\xi} = 0.265$ lead to a poorer fit. For the mixed substances the additional parameter N had to be considered to describe that part of the Tb contribution to the birefringence that is not proportional to the distortion e_A. The result of the fit for x = 0.4 at λ = 633 nm and the separation of the Tb contribution is shown in figure 7. The fitting parameters are listed in table 3. For x = 0.1, a good agreement with the measurements was obtained with the same parameters as for pure $DyVO_4$. Changes of $\tilde{\xi}$ or inclusion of a Tb contribution led to a less satisfactory fit. For higher concentrations x it was necessary to include a Tb contribution. The Tb levels were taken to be independent of temperature for x = 0.2 and x = 0.3, because here no Γ_3^+ phase transition occurs. For x = 0.4 the temperature dependence of the Tb levels had to be considered. They were calculated in MFA with the same parameters (half-width of the Γ_3^+ pre-strain distribution) as used in the calculation

for the Γ_3^+ transition. Thus the birefringence δn_A is the combined result of the consequences of the Γ_4^+ distortion and of the occupation numbers of the Tb^{3+} levels depending on the Γ_3^+ distortion. Despite this, the measurement of δn_A is not influenced by the birefringence δn_X except in the blue region of the spectrum.

The Tb contribution $x(e_A/e_0)p_1N$ to the birefringence according to equation (16) is shown in figure 7(*a*) by the broken curve. In figure 7(*b*) it is separated into the two temperature-dependent factors, the relative population p_1 and the distortion e_A/e_0. Their product yields the nearly straight course of the Tb contribution for $3\ K < T < 5\ K$. For $T < 2.6\ K$ the calculated and measured curves for $x = 0.4$ diverge (see figure 7(*a*)). To explain this, one could think of fluctuations in the concentration, which would lead to changes in the occupations of the Tb^{3+} levels as a consequence of locally differing Γ_3^+ distortions. These fluctuations would cause an additional broadening of the phase transition. The observed broadening, however, can be explained with fluctuations in the concentration x of $\Delta x \simeq 0.005$. This value is much too small to explain the difference between the curves for $T \leqslant 2.6\ K$. Magnetic effects—the high-temperature tail of the magnetic phase transition or consequences of internal magnetic fields from dipolar and exchange interactions—are ruled out in the same way. Furthermore, the agreement of calculated and measured curves gets less convincing with increasing magnetic field for all concentrations. This was observed already for pure $DyVO_4$ [17, 29]. An explanation has not been found so far.

As was already mentioned in paper I, the compressibility $\bar{\xi}$ as a function of the concentration, determined from the birefringence data, is approximately independent of x with a slightly higher value for $x = 0.4$ (see table 3 of I). This is in contrast to the specific heat and spectroscopic data, where $\bar{\xi} \sim (1 - x)^2$ was found (table 3 of I). For the birefringence higher values of $\bar{\xi}$ are necessary to explain the slope of the measured curves near the phase transition. For a more detailed discussion of this problem, see paper I.

5. Summary

The structural phase transitions in the mixed Jahn–Teller system $(Tb_x,D_{1-x})VO_4$ were investigated by means of birefringence measurements at different wavelengths in the visible part of the spectrum. To a first approximation the different contributions to the birefringence are proportional to the order parameter (distortion). But care has to be taken for parts of the spectrum where the total birefringence is very small. Here higher-order contributions may be effective.

For the Tb-rich crystals including pure $TbVO_4$, depending on concentration and wavelength, systematic deviations of the measured birefringence from the calculated mean-field distortion e were observed. The measured curves are not proportional to each other for different wavelengths. This could be explained by an additional contribution to the birefringence, which is proportional to the third power of e.

For the Dy-rich crystals the measured curves of the birefringence are proportional for different wavelengths. For pure $DyVO_4$ the experimental temperature dependence is reproduced well by the calculation of the order parameter, using the compressible Ising model [17]. With increasing dilution the calculated curves deviate from the measured temperature dependences, which to some extent could be explained by a contribution of the Tb^{3+} ions to the birefringence.

Acknowledgments

The author wishes to thank Professor A Kasten for stimulating this work. He also thanks him and Professor H G Kahle for many helpful discussions.

References

[1] Hess G, Dammann M, Kahle H G, Kasten A, Seifert C and Vögtlin K 1989 *J. Phys.: Condens. Matter* **2** 1073
[2] Ferré J and Gehring G A 1984 *Rep. Prog. Phys.* **47** 513–611
[3] Gehring G A 1977 *J. Phys. C: Solid State Phys.* **10** 531–42
[4] Gränicher H and Müller K A 1971 *Mater. Res. Bull.* **6** 977–88
[5] Hess G, Hikel W and Kahle H G 1989 *J. Phys.: Condens. Matter* **2** 1113
[6] Hintzmann W and Müller-Vogt G 1969 *J. Crystal Growth* **5** 274–8
[7] Gehring K A and Rosenberg H M 1971 *Phys. Status Solidi* b **47** K75–8
[8] Ellis C J, Gehring K A, Leask M J M and White R L 1971 *J. Physique Coll.* **32** C1 1024–5
[9] Kasten A and Becker P J 1973 *Int. J. Magn.* **5** 157–60
[10] Leask M J M, Maxwell K J, Tyte R N, Becker P J, Kasten A and Wüchner W 1973 *Solid State Commun.* **13** 693–5
[11] Kasten A, Berndts P and Kahle H G 1975 *Physica* **80B** 258–68
[12] Kemp J C 1969 *J. Opt. Soc. Am.* **59** 950–4
[13] Becker P J, Kahle H G and Keller E 1985 *Phys. Status Solidi* b **130** 191–6
[14] Pilawa B, Hess G, Kahle H G and Kasten A 1988 *Phys. Status Solidi* b **145** 729–39
[15] Becker P J and Gehring G A 1975 *Solid State Commun.* **16** 795–8
[16] Glynn T J, Harley R T and Macfarlane R M 1977 *J. Phys. C: Solid State Phys.* **10** 2937–46
[17] Gehring G A, Harley R T and Macfarlane R M 1980 *J. Phys. C: Solid State Phys.* **13** 3161–74
[18] Hess G 1988 *Doctoral Thesis* Universität Karlsruhe
[19] Elliott R J, Harley R T, Hayes W and Smith S R P 1972 *Proc. R. Soc.* A **328** 217–66
[20] Harley R T and Macfarlane R M 1975 *J. Phys. C: Solid State Phys.* **8** L451–5
[21] Wood I G and Glazer A M 1980 *J. Appl. Crystallogr.* **13** 217–23
[22] Kleemann W, Schäfer F J and Nouet J 1979 *Physica* **79B** 145–55
[23] Schäfer F J, Kleemann W and Tsuboi T 1983 *J. Phys. C: Solid State Phys.* **16** 3987–4002
[24] Borsa F, Bernard D J, Walker W C and Baviera A 1977 *Phys. Rev.* B **15** 84–94
[25] Bosch G, Jahn I R, Prandl W and Verhein M 1986 *Physica* **142B** 320–7
[26] Hikel W, Hess G and Kahle H G 1989 *J. Phys.: Condens. Matter* **1** 2137–40
[27] Kasten A 1980 *Z. Phys.* B **38** 65–76
[28] Page J H, Smith S R P, Taylor D R and Harley R T 1979 *J. Phys. C: Solid State Phys.* **12** L875–81
[29] Page J H, Taylor D R and Smith S R P 1984 *J. Phys. C: Solid State Phys.* **17** 51–71